



Recycling of waste toner derived from exhausted printer cartridges as adsorbent for defluoridation of water

Diksha Choudhary^{a,b}, Sapna Kaithwas^b, Kamlesh^{a,b}, R.K. Sharma^c, Alka Mishra^{a,b}, Sandeep Singh^{a,b}, Satvasheel Powar^{d,e,*}, Archana Singh^{a,b,**}

^a Academy of Scientific and Innovative Research (AcSIR), Ghaziabad 201002, India

^b Centre for Advanced Radiation Shielding and Geopolymeric Materials, CSIR-Advanced Materials and Processes Research Institute, Bhopal 462026, India

^c Technical Physical Division, Bhabha Atomic Research Center Trombay, Mumbai 400085, India

^d School of Mechanical and Materials Engineering, Indian Institute of Technology Mandi, Kamand, Himachal Pradesh 175005, India

^e School of Technology and Business Studies, Energy Technology, Högskolan Dalarna, Falun 7918, Sweden

ARTICLE INFO

Keywords:

Printer Cartridge Toner (PCT)
Fluoride
Adsorption
Water treatment

ABSTRACT

Due to the broad adoption of electronic and electrical equipment and the quick advancement of contemporary innovations in this domain, significant amounts of electronic waste have been produced. This category of waste includes the toner powder used by printers, copiers, and fax machines to print text and images. This paper describes a sustainable and environmentally friendly method of recycling waste toner powder. The chemical composition of this printer cartridge toner (PCT) powder is carbon, Fe_3O_4 , polypropylene (polymeric resin), and SiO_2 composite. Toner powder from exhausted printer cartridges was utilized as an adsorbent to remove fluoride from water. It has a fluoride adsorption capacity of 60 mg/g and a specific surface area of 20 m²/g. X-ray diffraction and electron microscopic investigations were used to investigate the chemical composition, structure, and surface morphology of the material. To analyze the collected experimental data, the Freundlich and Langmuir adsorption isotherm models were used. Time-dependent kinetic experiments were conducted to determine the mechanism of the adsorption process using pseudo-first-order kinetics, pseudo-second-order kinetics, and intraparticle diffusion kinetic models. The fluoride adsorption process was shown to be feasible and spontaneous ($\Delta G < 0$) based on calculated thermodynamic characteristics, which included enthalpy, Gibbs free energy, entropy ($\Delta S > 0$), and adsorption activation energy. The study also discussed its reusability as an adsorbent and examined its functioning capability in actual water.

1. Introduction

The demand for electrical and electronic gadgets has been expanding rapidly as a result of urbanization, industrialization, and population expansion. Electronic appliances, such as housing electrical appliances and IT/telecommunications devices, have become indispensable to everyday life. They produce a significant quantity of "e-waste"; according to the worldwide e-waste monitor, 53.6 Mt

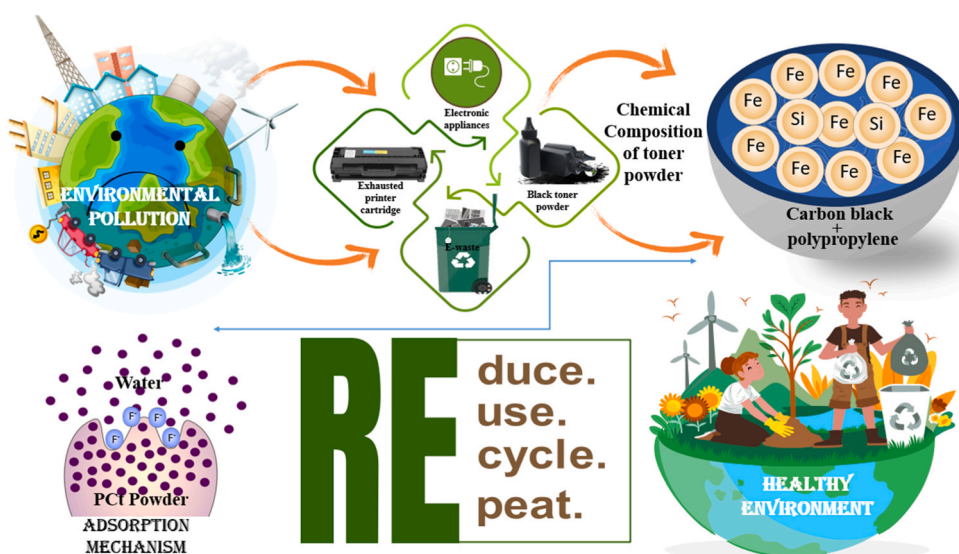
* Corresponding author at: School of Mechanical and Materials Engineering, Indian Institute of Technology Mandi, Kamand, Himachal Pradesh 175005, India.

** Corresponding author at: Academy of Scientific and Innovative Research (AcSIR), Ghaziabad 201002, India.

E-mail addresses: spw@du.se (S. Powar), archanasingh@ampri.res.in (A. Singh).

of e-waste was produced in 2019 (Parthasarathy, 2021). There are several e-waste categories that require care that wind up in landfills unrecycled. Even with the current digitalization trend, printers and ink cartridges remain a major source of electronic waste. On a global scale, ten lakh printer cartridges are discarded each day (Babar et al., 2019). Initially toner production process included; plastic slabs that were broken up and pulverized into powder during toner production. However, this led to uneven-sized particles that failed to stick to the paper well. In the toner hopper, they agglomerate and make inhomogeneous powder. To solve that problem producers, develop toner particles of a homogeneous size, which improves printed pictures and maximizes the usage of toner. The toner contained within cartridges is a patent composition unique to each printer maker, but the fundamental toner components, though, are not a big mystery – they are simply carbon black, iron, and a polymer as a binder. In addition to these chemicals, both black and color toners contain fumed silica and charge control agents. Fumed silica enhances the flow capacity of solids within the toner cartridge, reducing clumping and speeding up the printing process. Charge managing agents, such as magnesium, zinc, or large amounts of magnetic iron, are added to the powder particles to keep them charged, which is necessary for laser printing. As a consequence, there would be 26 kg of garbage from precious metals, 3000 tons of plastic waste, 2500 tons of waste from ferrous metals, and 400 tons of waste from aluminum (Dong et al., 2017). Each cartridge contains approximately 8% unused toner by weight, which releases 5443 metric tons of carbon powder into the environment (Akilarasan et al., 2018). Negligence in toner waste treatment, recycling, and reuse is predicted to cause severe environmental difficulties in the near future. It is critical to develop workable solutions for the recycling and reuse of toner waste in light of the present and future global contexts. Nonetheless, new opportunities for reusing and recycling toner waste are emerging. Previously, some research has been reported on converting waste toner carbon into potentially valuable compounds such as magnetic Fe_3O_4 extraction from toner powder, organic dye removal adsorbent, and sodium battery application material, etc. (Arjunan et al., 2021; Nazlan et al., 2022). Hong Zhu and colleagues removed Cr(VI) by decomposing waste toner at high temperatures and calcining in different atmospheres (Zhu et al., 2018). Following that we used printer cartridges toner (PCT) powder for water contamination treatment.

As an essential element of life, water serves as the foundation for the environment. This ecosystem's component has suffered significant issues and is no longer sufficient to be used as drinking water due to the recent fast rise in both the human population and industry. More than half of the world's population relies on groundwater for drinking purpose which was getting contaminated day by day because of rapid growth of industries (Choudhary et al., 2022). Consumption of contaminated water can cause numerous health problems. According to WHO guidelines, the ideal fluoride level in drinking water that is safe to consume is between 0.5 and 1.0 mg/L, the higher concentration of fluoride tends to numerous health problems (Choudhary et al., 2023). Fluoride levels above 1 mg/L are consumed by more than 200 million people worldwide (Kouser et al., 2022). Fluoride contamination is therefore viewed as a serious problem when it comes to providing clean drinking water. Hence, high fluoride concentration in drinking water is necessary to treat, therefore various methods such as ion exchange, membrane separation, electrolytic defluoridation, electro-dialysis, and adsorption were used to treat fluoride from water (Solanki et al., 2022). Among these methods, adsorption is one of the most widely applied methods for removing fluoride ions from water. Due to its affordability and good results. Numerous synthetic metal oxides, both single and multi-component, and carbon-based materials, including composites of nickel oxide, aluminum oxide, magnesium oxide, and carbon nanomaterials, have been reported to date (Solanki et al., 2019). Because of the synergistic interactions between the constituent species, the majority of the reported composites were carbon-based materials and metallic oxides based on iron or aluminum, which had greater adsorption properties (Solanki et al., 2020). Since PCT powder contains all the properties of good adsorbents like the amount of carbon, iron, and some metal oxides, therefore it became an ideal example of recycletion process of waste material, and a cost-effective process of water treatment. In view of this, we planned to successfully use PCT into value-added adsorbent for water



Scheme 1. Schematic representation of the study.

treatment. The objective of this work was to evaluate the adsorption capacity of PCt powder as an adsorbent for the elimination of fluoride from aqueous solutions. The study also investigated the influence of several parameters, such as the dosage of adsorbent, the pH of the solution, and the content of fluoride in the water. The Freundlich and Langmuir isotherm models were employed for the determination of the fluoride adsorption capacity, with the Langmuir model exhibiting the most favorable agreement. The temperature dependence of adsorption necessitates the assessment of thermodynamic parameters to ascertain the viability and spontaneity of the adsorption process inside the system. The study presents a thorough thermodynamic analysis, as well as information on how it performs in real water and its reusability as an adsorbent. The use of positively charged PCt for negatively charged fluoride ions removal is the first ever reported. This recent study has concentrated on producing value-added materials from waste toner without polluting the environment. [Scheme 1](#) shows the overall story of this article.

2. Experimental section

2.1. Materials

The powder material was extracted from used exhausted printer cartridges (12 A type). All of the chemical reagents used in this work, such as sodium hydroxide (NaOH), sodium fluoride (NaF), and sulfuric acid (H₂SO₄), were bought from Sigma Aldrich and used without additional purification. All experiments were carried out in deionized water.

2.2. Materials characterization

The substance's precise composition was determined by conducting X-ray fluorescence spectroscopy (XRF) using a Bruker India Scientific XRF Model S8 Tiger and powder samples placed on a 40 mm diameter pallet. Diverse sophisticated analytical techniques were employed to ascertain the morphological and physicochemical characteristics of the materials. The investigation of the materials' crystalline phase was conducted utilizing a Bruker AXS with D8 advance and a Cu K α radiation source ($\lambda = 1.5406$). The Bruker Alpha II spectrometer was used to record Fourier transform infrared (FTIR) spectra. The Raman spectrum was obtained with Technos equipment, namely the IndiRam CTR-300 model, equipped with a 20X lens and a 100-mW laser. The NOVA touch LX4 instrument was employed to determine the surface area and pore volume of the material by the N₂ adsorption-desorption isotherm technique. The morphology of the materials is examined using field emission scanning electron microscopy (FESEM). The X-ray photoelectron spectroscopy (XPS) examination was conducted utilizing a Thermo Fisher Scientific-Nexsa surface analysis spectrometer that has a micro-focused, monochromatic Al K (1486.7 eV) X-ray source.

2.3. Batch studies

The fluoride removal process was investigated using the batch adsorption approach. The fluoride solution was made by combining sodium fluoride (NaF) with deionized (DI) water. The experiment was to mix 100 mg/L of fluoride solution with 0.2 g of PCt powder in a 250 ml conical flask. The experiment was conducted under neutral circumstances with a pH of 7. Subsequently, the flask was positioned in a rotary shaker and subjected to a speed of 150 revolutions per minute for a duration of 60 minutes. Subsequently, the material and solution were segregated, followed by the utilization of a spectrophotometer to ascertain the ultimate fluoride concentration. The equation provided was utilized to ascertain the fluoride adsorption capability of the material:

$$q_e = (c_0 - c_e) V/m \quad (1)$$

Where q_e stands for a material's adsorption capacity, C_0 for the material's initial fluoride concentration (mg/L), C_e stands for the material's final fluoride concentration (mg/L), V for the solution's volume (liter), and m for the material's mass (gram).

The fluoride concentration was double-checked by Indian Standard guideline IS: 3025-60 (2008). The fluoride removal percentage was calculated using the following equation:

$$R\% = ((c_0 - c_e)/c_0) \times 100 \quad (2)$$

The adsorption isotherm was used to better understand the adsorption process. The Langmuir adsorption isotherm is a popular model for explaining adsorbate-adsorbent equilibria.

2.4. Column studies

The fixed bed column study was carried out for the investigation of the material's industrial-level performance. For this experiment, a borosilicate glass column with a 25 mm diameter and 350 mm length was filled with sand, cotton, and PCt material. In this experiment, a 3-ppm fluoride concentration was taken. Because this will provide more practicality being applicable at the industrial level. In this experiment, the flow of water was kept downwards from the top of the column, and treated water was collected from the bottom of the column. Thereafter samples were collected at certain intervals to analyze the fluoride concentration. This experiment was done till its concentration reached 99% of its initial concentration.

3. Results and discussion

3.1. Elemental composition

The XRF analysis of PCt materials before fluoride uptake revealed that the sample's main elemental components are Fe_3O_4 , and SiO_2 , with traces of other elements, like magnesium, aluminum, iron, and zinc. According to pre-reported literature printer cartridge black toner powder has 35–40% carbon in it. The obtained waste toner powder results show a high iron oxide (magnetite) content (Table 1). Because XRF can't measure the amount of carbon, here in the table only metal oxide amount in % is mentioned (Fernández et al., 2022).

3.2. Structural characterization

To better understands materials chemical and physical properties, its further characteristic study was done and mentioned below.

The X-ray diffractogram in Fig. 1(a) clearly indicates magnetic Fe_3O_4 to be the dominant crystalline phase in the toner powder. The diffraction peaks at $2\theta = 30.1^\circ, 35.4^\circ, 43.0^\circ, 53.4^\circ, 56.9^\circ$, and 62.5° were indexed to the cubic structure of Fe_3O_4 as confirmed by JCPDS 19-0629 (Zhu et al., 2018). It has a cubic inverse spinel group structure with space group of $\text{Fd}3\text{m}$ (227). Since it has a cubic structure its cell parameters are $a=b=c=8.39$ and its angles are $\alpha=\beta=\gamma=90^\circ$. It has the structure $[\text{Fe}^{3+}]_A[\text{Fe}^{2+}\text{Fe}^{3+}]_B\text{O}_4$, where A is the tetrahedral and B is octahedral, where this unit cell contains 32 Oxygen in a close-packed FCC (face-centered cubic) structure. Other components like SiO_2 (JCPDS No. 29-0085) and carbon black (JCPDS 41-1487) are found at planes (220) and (311) (Lou et al., 2013; Peng et al., 2013). As XRF results confirmed PCt has Fe_3O_4 , SiO_2 , and carbon black. The broad peak at plane (002) represents the amorphous organic residue of the toner powder (i.e., the polymeric resins) with an amount of very low SiO_2 (Dong et al., 2017).

Since the PCt powder has organic contents in it confirming the type of unequivocal identification of the polymeric composition is difficult. Therefore, by FTIR analysis it is possible to identify various functional groups present in the PCt powder. In this view, the FTIR spectroscopy was recorded in the range of $400\text{--}4000\text{ cm}^{-1}$. Fig. 1(b) shows the presence of band at 3024 cm^{-1} appears due to CH_2 asymmetrical stretching vibrations (Yordanova et al., 2014). The band at 2841 cm^{-1} and 2910 cm^{-1} corresponds to symmetrical stretching of CH_3 and CH_2 (Kumar et al., 2018). Another band at 1722 cm^{-1} and at 1597 cm^{-1} corresponds to the $\text{C}=\text{O}$, stretching vibrations of the carboxyl group (Pirela et al., 2015). The bands at 1447 cm^{-1} , and 1373 cm^{-1} appear due to the absorption vibration of C-H stretching and deformation vibrations of the C-H group respectively. The band at 1147 cm^{-1} is a characteristic of C–O–C stretching vibration in the repeated $-\text{OCH}_2\text{CH}_2-$ unit. The band at 1067 cm^{-1} corresponds to the Si–O bonding of SiO_2 . The C–O stretching is linked to the intensity of the peaks at 1024 cm^{-1} , and the existence of carbon and oxide may cause the C–O–C symmetric stretch, which is responsible for the band at 903 cm^{-1} (Itoua et al., 2023). The band at 747 cm^{-1} is caused by OH vibrations, whereas the band at 562 cm^{-1} is caused by the Fe–O bond of Fe_3O_4 . The presence of organic compound in the material is confined as polypropylene ($(\text{C}_3\text{H}_6)_n$), its mixed in toner powder as binding material (Hammani et al., 2019). Other notable thing is C–C bonds in spectra, they correspond to the presence of carbon black in toner powder.

Fig. 1(c) shows the Raman spectra of PCt powder, this spectrum initially has three bands at 190 cm^{-1} , 338 cm^{-1} , and 479 cm^{-1} , which corresponded to the vibration modes of Fe–O bonds of Fe_3O_4 (Hai et al., 2008). The spectra showed a peak at 1278 cm^{-1} that indicated the D-band of Fe_3O_4 (Hai et al., 2008). The band at 883 cm^{-1} and 995 cm^{-1} corresponds to polypropylene. Figure S1 shows band at 1354 cm^{-1} and 1582 cm^{-1} corresponds to carbon black (Koochakzaei et al., 2022). All the data of Raman spectra confirms the presence of carbon and magnetic iron composite in it, which has good agreement with other characteristic data.

Fig. 1(d) displays the nitrogen adsorption-desorption isotherm of PCt, as indicated by BET data. The adsorption capacity of PCt has shown a gradual rise throughout the P/P0 range of 0.2–0.8, indicating the presence of mesopores. The PCt material exhibits a pore diameter distribution centered at 2.7 nm, as indicated by the pore size distribution obtained using the Barrett-Joyner-Halenda (BJH) model (Fig. 1(d) inset). This finding closely aligns with the literature findings. PCt has a pore volume of 0.004 cc/g and an estimated total specific surface area of $20\text{ m}^2/\text{g}$. It is important to note that PCt's surface area and mesoporous properties enhance the adsorption process. Further, the physical characteristics of PCt are summarized in Table 2.

The morphology of the adsorbent was studied using the FESEM (Fig. 2(a, b)). The adsorbent's surface morphology shows a cotton-like structure with many spheres and a rough surface with numerous bumps on the surface (Kaipannan et al., 2019). Additionally, the elemental mapping studies and EDAX spectra of the PCt material confirmed the existence of C, Fe, O, and Si (Au because of coating on

Table 1
XRF Analysis (Major Oxides in Waste Toner Powder (PCt)).

Compound	Amount (%)
Fe_3O_4	86.6%
SiO_2	10.25%
MgO	1.2%
Mn_3O_4	0.2%
CaO	0.4%
Al_2O_3	0.45%
SO_3	0.5%
ZnO	0.3%

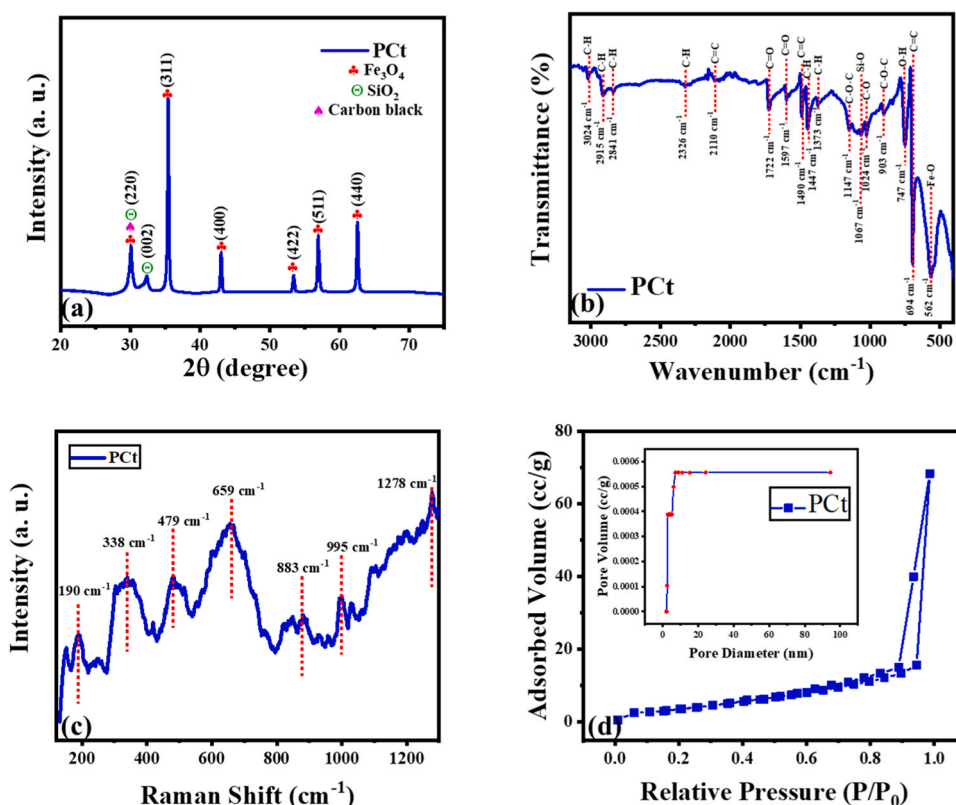


Fig. 1. PXRD patterns (a), FTIR spectra (b), Raman spectra (c), and N_2 adsorption–desorption isotherm (d) and inset pore size distribution of PCt.

material) elements on the material surface (Fig. 2(c)). To learn more about the distribution of C, Fe, O, and Si in the matrix as seen in Fig. 2(d) and (e), respectively, X-ray elemental mapping of the PCt material (Fig. 2(d–i)) was carried out. The presence of carbon ferric composite is confirmed by the intermixed distribution of the elements carbon, iron, silica, and oxygen.

3.3. Adsorption results

The fluoride adsorption capacity of PCt was assessed at an initial fluoride concentration of 100 mg/L, and experimental results show that the capacity is 60 mg/g towards fluoride. ICP-MS testing was done on this solution to ensure that there was no elemental leaching present (Table S1). To investigate its overall potential towards fluoride ions, additional experiments such as isotherm, kinetic, and thermodynamic studies were carried out.

3.4. Variations in the fluoride concentration and adsorption isotherm

To examine material performance in different fluoride concentrations, this study was done and with these results, its isotherm's parameters were also calculated to further know about material's maximum adsorption capacity. To perform these experiments, we took fluoride solution in the range from 10 to 100 mg/L, with 0.02 g/L mass, and shaken for 60 minutes at neutral pH. The percentage of adsorption considerably decreased as the initial fluoride concentration rose (Fig. 3).

Fig. 3(a, b) reveals that when the fluoride concentration was increased, the removal efficacy of the adsorbent material decreases. The current behavior is caused by increased fluoride concentration, which fills all active sites of adsorbent material. Between the surface of the adsorbent and the adsorbate, the adsorption process establishes a dynamic equilibrium (Raghav and Kumar, 2018).

Table 2
Physical properties of PCt sample.

Physical Characterization	PCt powder
Particle shape	Cotton-like structure with spheres
BET surface area	20 m ² /g
Average pore diameter	2.7 nm
Pore volume	0.04 cm ³ /g

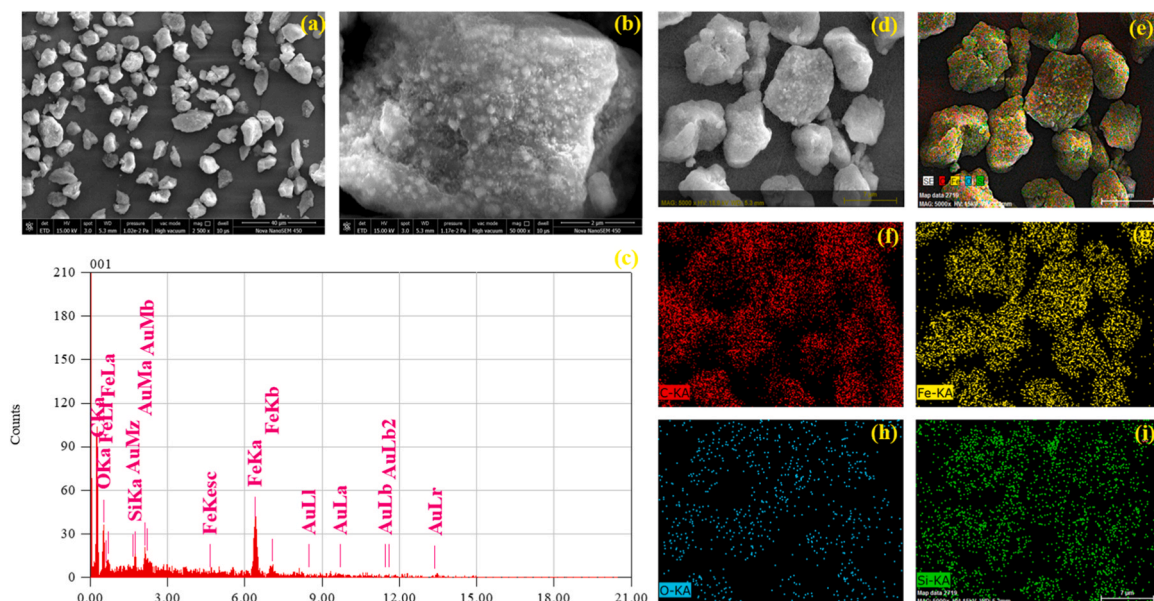


Fig. 2. (a-b) Surface micrographs of PCt powder at different magnifications, (c) EDAX spectra, and (d-i) mapping of the C(carbon), Fe(iron), O (oxygen), and Si (silica) elements respectively.

Adsorption isotherms like Langmuir and Freundlich isotherms are the widely used adsorption models for studying the mechanism of the adsorption process.

The maximum adsorption capacity (q_m) obtained by fitting experimental data to Langmuir equations was found to be 65 mg/g (Table 3). The correlation coefficient (R^2) is 0.99, and the value of R_L in this study is 0.9, indicating that fluoride adsorption on PCt particles is favorable in nature. The Langmuir equation can adequately explain this adsorption process, as shown by the fact that the

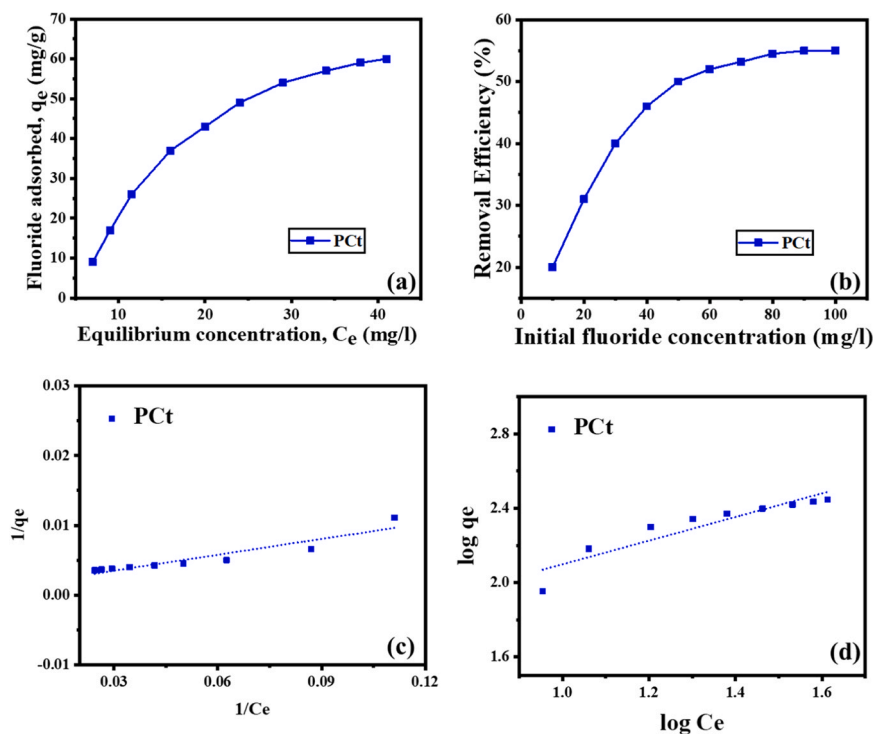


Fig. 3. shows the equilibrium concentration and adsorption capacity in (b) and the initial concentration of fluoride vs removal % in (a). Adsorption curves for the Freundlich and Langmuir isotherms (c, d) of the PCt, respectively.

correlation coefficient (R^2) obtained from the Langmuir model is greater than that obtained from the Freundlich model. The adsorption capacity K_f for the Freundlich isotherm is not very near to the experimental value because it depends on the adsorbate and adsorbent's properties. The nonlinear parameter n represents the heterogeneous energy of the adsorption surface. In our case, the Freundlich equation was satisfied if $1/n < 1$, which indicates that the adsorption is likely to be successful.

3.5. Effect of adsorbent dose

PCt powder doses of 0.2, 0.4, 0.6, 0.8, 1.0, and 1.2 g/L were used to study about how much amount of adsorbent should be suitable for specific concentration of fluoride. To perform this experiment 100 mg/L of fluoride with 100 ml volume was shaken at 150 rpm in neutral condition, with a contact time of 60 minutes. The effects of PCt adsorbent dosages on fluoride uptake are shown in Figure S2. The graphs demonstrate that as the adsorbent dosage was increased from 0.2 to 1.2 g/L, the removal efficiency of fluoride rose quickly. Further increases in material dose did not significantly boost the elimination of fluoride. The enhanced fluoride removal capacity could have been caused by the increased material dose, which may have resulted in more sorbent surfaces or active sites for fluoride uptake (Rathore and Mondal, 2017). But beyond a certain point, it stops showing an upward trend since the amount of fluoride ions present is the same but the number of active sites is greater; as a result, after 0.08 g of adsorbent, a straight line is visible.

3.6. Impact of contact time and adsorption kinetics

The performance of the material's adsorption is also influenced by the contact time. To study more about, how much time is sufficient for the better fluoride adsorption into PCt, experiments were done in the time range of 20–120 minutes. The tests were done with 100 mg/L of fluoride, a pH of 8, and a mass of 0.02 g/L (Fig. 4(a)). For porous solid adsorbents, the total adsorption rate is determined by how well the adsorbate molecules can get inside the particle. The process of adsorption was studied to find out how fast and where the adsorption happened up to equilibrium. The pseudo-first-order model, the pseudo-second-order model, and the intra-particle diffusion model were all used to show how the adsorption happened (Fig. 4).

Fig. 4(a) demonstrates that fluoride adsorption onto PCt occurs quite quickly and reaches equilibrium in less than 120 minutes, suggesting that the mesoporous structure and positively charged surface would speed up this process due to electrostatic attraction. The experimental results and calculated data in Fig. 4(b) and (c) demonstrate that the pseudo-second order model best fitted for fluoride removal. The theoretically calculated adsorption capacity $q_e = 67$ mg/g, was very close to the experimental value $q_e = 60$ mg/g. Another important factor is the linear fitting coefficient ($R^2 = 0.99$) of this graph shows high value when comparing to pseudo first order model (Table 4).

To learn more about the adsorption rate, the kinetic data was fitted to the intra-particle diffusion model (Fig. 4(d)). The results show that fluoride adsorption on PCt occurs in two steps, the first slope is sharp compare to second, indicating that initial slop is more responsible for fast adsorption process and remaining process occurs in second step. Based on published data, it has been shown that the initial linear slope corresponds to a rapid diffusion process occurring due to boundary effects, while the subsequent linear slope represents a slower attainment of equilibrium resulting from intra-particle diffusion processes. The high fitted correlation coefficients of R^2 (0.99) indicate a strong relationship between fluoride adsorption and the intra-particle diffusion model. This suggests that the adsorption process of fluoride onto PCt can be better explained by the intra-particle diffusion model, as shown in Table 5.

Fluoride's higher K_d value ($1 \text{ mg/g/min}^{1/2}$) indicated a more rapid diffusion into PCt's mesoporous structure. It showed a stronger boundary layer effect at first slope (i.e., molecular diffusion in solution) during the adsorption of fluoride by PCt.

3.7. Impact of the solution's pH

Another key aspect is pH of the solution which directly affects the absorption process of adsorbent materials. In order to better understand the adsorption mechanisms in both acidic and basic environments, further experiments from pH range 4–9 were performed with 0.2 g of adsorbent dose and initial fluoride concentration of 100 mg/L, and contact period of 60 minutes at room temperature. The adsorbent's surface charge and the pollutant's solution phase chemistry both play essential roles in the adsorption process. Since groundwater normally has a pH between 6 and 8, the aforementioned pH range was taken into consideration (Fig. 5(a)).

The point of zero charge value (pH_{PZC}) of adsorbent material is essential to the adsorption process. The pH_{PZC} value of adsorbent indicates that the adsorbent surface's net charge is zero. When the pH of the solution falls below pH_{PZC} , the adsorbent's net surface charge on the solid surface becomes positive due to excess of H^+ ions, which is advantageous for fluoride adsorption because fluoride is a negatively charged ion that is deemed to show coulombic attraction. In this case, the PCt has neutral response around pH 7.5, suggesting that the surface of the material is positively charged below this, which facilitates fluoride ion adsorption at lower pH levels (in the presence of H^+ ions). Fig. 5(b) demonstrates how the percentage of fluoride adsorption reduces as the pH of the solution rises because the fluoride is repelled by the adsorbent's surface negative charge (rising OH^- ions). Similar findings have been reported in the

Table 3
Isotherm parameters for fluoride adsorption on PCt.

	Langmuir model				Freundlich model		
	q_m	R^2	b_L	R_L	$1/n$	K_f	R^2
PCt	65 mg/g	0.99	2.57	0.98	0.64	47	0.95

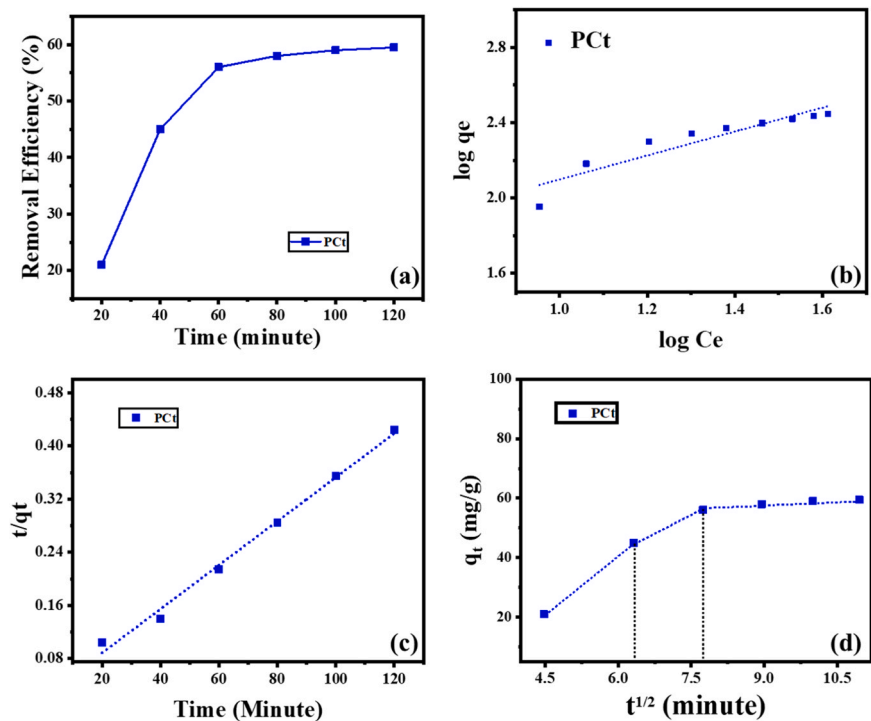


Fig. 4. Adsorption experiment with varying contact periods (a). Pseudo-first-order (b) and pseudo-second-order (c) fluoride adsorption kinetic fits, as well as an intraparticle diffusion graph (d).

Table 4
Parameters of pseudo-first-order and pseudo-second-order kinetic models.

Pseudo-first-order model				Pseudo-second-order model		
PCt	K_f	q_e	R^2	K_s	q_e	R^2
	0.08	49 mg/g	0.93	0.0057	67 mg/g	0.99

Table 5
Parameters for intraparticle diffusion of PCt.

Intraparticle diffusion	K_d (mg/g/min ^{1/2})	R^2	Temperature (K)
PCt	1 mg/g/min ^{1/2}	0.999	303

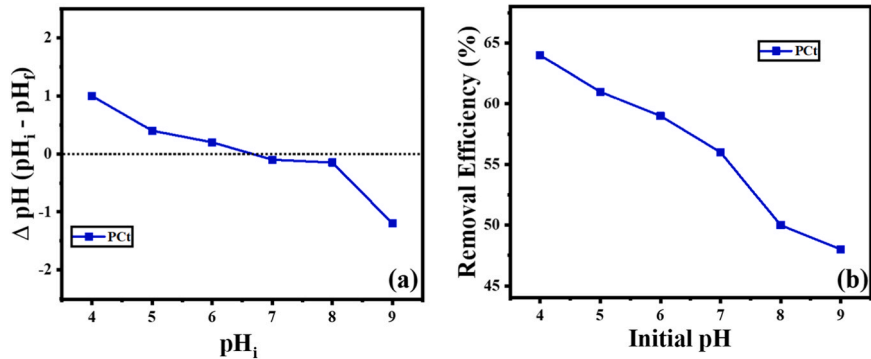


Fig. 5. ΔpH curve of PCt (a) and varying pH effect on the removal of fluoride (b).

literature, where the increased fluoride absorption at lower pH was attributed to the electrostatic attraction process. Although water's pH typically has a neutral value, we conducted all of our experiments at pH 7.

3.8. Adsorption thermodynamics

A thermodynamic study was done to determine the adsorption capacity at various temperatures, despite the fact that temperature affects the adsorption process. On the other hand, room temperature reactions are more useful in investigations of contaminant removal. The purpose of this study was to learn more about the effects of temperature throughout the year. For the adsorption experiments, three different temperatures (303, 313, and 323) were used together with a starting fluoride concentration of 100 mg/L (at neutral pH with 0.02 g adsorbent dose and 60 min. contact period). Indicating that PCt interacts with fluoride at a little lower temperature, it appears that the adsorption capability steadily reduced as the temperature increased. [Table 6](#)

The study's results suggest that doing the adsorption process at lower temperatures, particularly at room temperature, offers more advantages. This finding is substantiated by the ΔG values acquired under three distinct temperature settings. The confirmation of the reaction's feasibility and the spontaneous nature of adsorption was achieved by the detection of a negative change in Gibbs free energy (ΔG) at a given temperature ([Raghav et al., 2018](#)). The correlation between temperature and the change in Gibbs free energy (ΔG), as explained in the section on activation energy, illustrates a decreasing trend in the viability of fluoride adsorption. The reported ΔH value of -14.7 kJ/mol supports the practicality and appropriateness of the adsorption approach, indicating that the interaction between fluoride and PCt may occur at a much lower temperature. The symbol ΔS represents the degree of affinity and unpredictability found at the boundary between a solid and a liquid, which aids in the adsorption process. This discovery is consistent with the previously published statistics. Physical adsorption is a phenomenon that causes a decrease in both the free energy and entropy of the adsorption system, resulting in an exothermic reaction.

3.9. Activation energy

An Arrhenius plot was created after the kinetic data had been collected and the rate constant for the reaction at the three distinct temperatures was identified. To determine the process's activation energy The log k_2 (adsorption capacity) vs. $1/T$ (temperature) plot is produced.

The values of E_a (activation energy) were determined from the slope of the plot presented in [Figure S3](#). The activation energy value helps to explain the mechanism whether the binding in adsorption occurs through physisorption or chemisorption. The activation energies for physical attraction are typically lower. While chemisorption has higher activation energies and requires more energy ([Raghav et al., 2018](#)). According to data from activation energy studies, fluoride ions onto the PCt binds through physisorption since its ions have activation energies under very low (less than 40 kJ/mol) at room temperature. The high fluoride affinity of PCt and the viability of the reaction are supported by the much lower value of the activation energy E_a (19.2 kJ/mol) mentioned in [Table 7](#).

3.10. Fixed-bed column adsorption study

The effect of fluoride concentration on material was studied with this method. For this experiment, PCt material was put into a column with sand and cotton on top and bottom to ensure ideal packing. This column has a bed length of 23 cm, 25 g of PCt material, and 250 μm homogeneous sand particles. The obtained results are mentioned in [Table 8](#), 3 ppm fluoride results show that it can treat large volume of fluoride water. these results indicate that lower fluoride concentration gives higher breakthrough time and larger V_{eff} value ([Talat et al., 2018](#)).

Because flow rate is a little higher it shows saturation on the material in the early stage, more contact time provides more reaction time. Although, 3 ppm concentration reaches its permissible limit after treating 9 liters of fluoride water. [Figure S6](#) shows the C_t/C_0 versus time (t) graph of fixed bed column studies at different fluoride concentrations. As can be seen from [Figure S6](#), column study data compliments the batch adsorption data in this study. In summary, we can say this could be used on a large scale to treat various concentrations, without elemental leaching.

3.11. Real sample analysis

A real groundwater sample collected from Himmatgarh Village, Dhar District, Madhya Pradesh, India, is utilized to evaluate the efficacy of the adsorbent in eliminating fluoride. The concentration of fluoride in the hand pump samples was measured to be 6.8 mg/L, exceeding the allowable limit by approximately sixfold. For the treatment of 100 ml of water, a quantity of 2 g of PCt material was utilized. The adsorbent effectively reduces the fluoride concentrations in drinking water to levels below the authorized limit set by the

Table 6
Thermodynamic studies of PCt for defluoridation.

Material	Temperature (K)	ΔG (kJ/mol)	ΔH (kJ/mol)	ΔS (kJ/mol)
PCt	303	-9.4	-14.7	0.97
	313	-10.3		
	323	-11.03		

Table 7
Activation energy parameters of PCt.

Materials	Activation energy (E_a) (kJ/mol)
PCt	19.2

Table 8
Adsorption data for fixed-bed PCt column for fluoride adsorption at 3 ppm fluoride concentration.

Initial fluoride concentration (Z= 23 cm), Q = 13 ml/min) 3 ppm	V _{eff} (ml)	t _b (min)	t _e (min)	q (mg/g)
	156,000	702	936	2.8 mg/g

* Z = Bed length, Q = flow rate.

World Health Organization (1.5 mg/L). [Table 9](#) displays the properties of the water samples before and after treatment, demonstrating strong evidence that the fluoride concentration reduced to levels that are considered acceptable after the treatment material was applied. The fluoride concentration in the groundwater sample is 1.2 mg/L. Another significant finding is that the TDS and conductivity of the treated water remain constant, suggesting that no ions from the adsorbent have transferred into the water. This is a vital factor for the adsorbent, particularly in its implementation for the purification of potable water.

3.12. Regeneration and desorption studies

The spent PCt powder was regenerated with chemical treatments such as dilute H₂SO₄ (1 M) and dilute NaOH (1 M) (as desorbent agents) followed by reported article of Choudhary and team ([Choudhary et al., 2023](#)). The regeneration studies were done at room temperature. The spent PCt powder was first dipped into the basic solution in 250 ml conical flask. The flask was then shaken for 60 minutes at room temperature with a thermomechanical shaker. After multiple washing, it was dipped into the acidic solution then the this PCt powder was washed several times with deionized water, and the resultant powder was heated in a hot air oven at 80 °C for 2 hours. After regeneration it was again used to treat fluoride from water, after every recharge it loses its original potential may because some pores of adsorbent get saturated and does not regenerate again. The desorption efficiency was calculated as the ratio of fluoride desorbed to adsorbed. Fluoride desorption levels ranged between 87% and 88% after its first regeneration. After three cycles, desorption efficiency decreased by 25–27%. The desorption mechanism, we believe relies on the principal of the ion exchange method. On the adsorbent surface, when the fluoride-saturated media is treated with 1 M NaOH, OH⁻ ions of the NaOH replaces the adsorbed fluoride ions, once the PCt surface gets OH⁻ saturate than the treatment with acid is done to make surface neutral so that adsorbent gets ready to remove more fluoride ions present in the walls. [Figure S5](#) depicts the desorption and reuse of PCt at fluoride concentration at 10 mg/L throughout three regeneration cycles. its adsorption capacity decreasing from 65% to 40%, during the three-regeneration process. Based on the regeneration results, PCt would be an efficient and cost-effective adsorbent material with good regeneration ability. As a result, the PCt will be reused for up to three regeneration cycles. PCt was applied after regeneration and demonstrated no leaching in water, demonstrating its stability and reproducibility ([Table S2](#)).

4. Characteristic analysis after adsorption

After fluoride adsorption materials characteristic analysis is very important aspect of the study, following that spent PCt powders morphology studies were carried out, in [Fig. 6](#).

As discussed, earlier PCt powder has cotton like structure, and sphere of Fe₃O₄. After fluoride adsorption it's does not shows any drastic morphological differences between bare and spent PCt powder. Its EDX results clearly shows that it has fluoride (marked in circle) on its surface, which supports successful adsorption of fluoride on PCt ([Figure \(c\)](#)). Its elemental mapping on spent PCt shows it has same chemical composition as bare PCt ([Figure \(d-i\)](#)), indication that, during adsorption process PCt powder has not loses its originality. After studying spent PCt morphology, its characteristic properties before and after adsorption was also studied which mentioned in [Fig. 7](#) to better understand the materials importance as adsorbent.

As can be seen from [Fig. 7\(a\)](#), XRD spectra of material before fluoride adsorption and after adsorption, which indicates that there is

Table 9
Raw water and PCt treated water parameter.

Parameters	Raw water	PCt Treated water
Fluoride Concentration (mg/L)	6.8	1.2
Electrical Conductivity (μS)	338	342
Total dissolved solids (mg/L)	248	251
pH	7.5	7.2

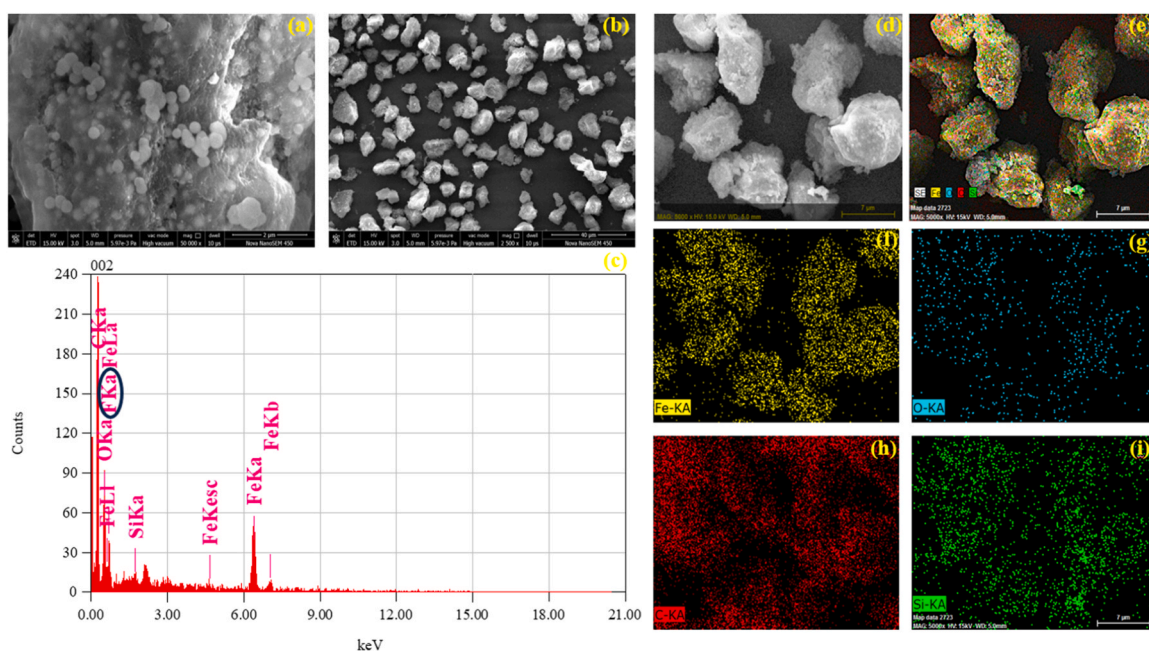


Fig. 6. (a-b) Surface micrographs of PCt powder at different magnifications, (c) EDAX spectra, and (d-i) mapping of the C(carbon), Fe(iron), O (oxygen), and Si (silica) elements respectively.

no major difference presented in it. This XRD spectrum is matched well with the reported literature. Furthermore, after fluoride adsorption, PCt XRD revealed that the broad peaks (plane 002) of organic residue have completely disappeared may due to the decomposition of polymeric resin in it, or can its reflections are missing after annealing because the grains are not oriented correctly to allow diffraction from these planes. To confirm polymeric resin involvement, FTIR data (Fig. 7(b)) of material before and after adsorption was compared. However, this data does not show any major difference in it, which is directly attributed to that its polymeric resin does not interrupt the adsorption process. Although its carbon silica and iron content remain as it is, which strongly supports that it did not leach anything during adsorption. In Fig. 7(c), Raman spectra of material before and after adsorption show that it's surface after adsorption changes a little due to the presence of fluoride ions on its surface, but does not support any chemical change. To confirm this X-ray photoelectron spectroscopy (XPS) measurements were performed to determine the chemical compositions and electronic structure of PCt, and a typical full XPS spectrum is shown in Fig. 7(d).

Fig. 7(d) shows the XPS survey spectra of bare or spent material. As shown in the wide scan XPS spectra, the characteristic peaks of the main elements (C, Fe, Si, O) of PCt were detected. Following fluoride adsorption, a new peak at 685 eV grew, which was attributable to the F 1s photoelectron. The appearance of a F 1s signal in spent PCt proved that the surface interaction between fluoride and PCt material was taking place. This strong F1s peak shows PCt has a huge amount of fluoride ions on its surface after adsorption. Figure S6 (a) displays the high-resolution Fe 2p spectrum. the Fe 2p_{3/2} and Fe 2p_{1/2} spin-orbit peaks, which are located at binding energies of 710.8 eV and 724.6 eV, respectively, indicate the formation of Fe₃O₄ (Bhaumik et al., 2011). The C 1s high resolution spectra (Figure S6 (b)) show peak at 284.6 eV corresponds to C-C bond of carbon black. The O 1s spectrum (Figure S6 (c)) shows binding energy at 533.1 eV corresponds to oxygen iron bond. After fluoride adsorption the binding energy of O 1s shifted a little may because presence of fluoride on PCt surface affect its position. In high-resolution XPS spectra (Figure S6 (d)), peak at 103 eV and 154 eV corresponded to Si 2p and Si 2s respectively, confirm the presence of SiO₂ in PCt. Hence its confirmed that bare and spent PCt powder has major part of carbon/iron composite in it (Saini et al., 2019). After adsorption PCt shows shifting in its characteristic peaks. This shift in XPS spectra occurs because increasing the electron density of an atom (such as fluoride ion compared with Oxygen) decreases the binding energy. To confirm this, Figure S7 compares the normalized O 1s spectra of the composite before and after fluoride adsorption. It is evident that there is a notable decrease in the intensity of O 1s peaks, indicating that fluoride in the water is exchanged with hydroxyl ions on the adsorbed surface, in accordance with Dhillon et al. (2016).

Table 10 shows the different adsorbents and their fluoride adsorption capacity (mg/g), which includes various metal oxides and carbon-based materials developed till date. This clearly indicates that our material shows excellent results without any synthesis efforts and costs.

The possible mechanisms of fluoride adsorption on PCt powder are depicted in Fig. 8. For the remediation of fluoride-containing water, metal oxides and hydroxides as well as their composites have received quite a bit of attention because they have positively charged surfaces that make it easier for negatively charged fluoride ions to be attracted to them via electrostatic attraction. It is worth noting that the majority of the literature on the adsorptive mechanism of fluoride focuses on the adsorbent surface. According to the reported hypothesis, Carbon black is insoluble in water, when mixed with metal oxides its water dispersibility increases, which gives more active site to fluoride for adsorption. Fluoride adsorption mechanism onto PCt is presented in Fig. 8.

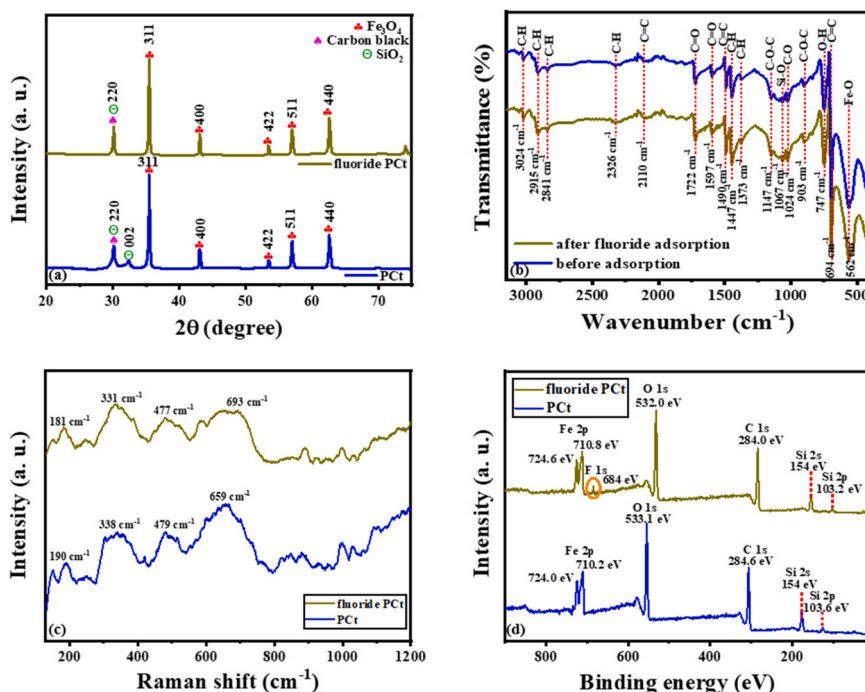


Fig. 7. PXRD patterns (a), FTIR spectra (b), Raman spectra (c), and X-ray photoelectron spectroscopy (XPS) spectra (d) of bare PCt and spent PCt.

Table 10

The adsorption capability of various metal oxide, carbon black/carbon-based materials, and metal-carbon composite material adsorbents used for fluoride removal is presented.

S no.	Adsorbent name/ Description	Adsorption capacity (mg/g)	Reference
1.	Nanoalumina-supported Mn_2O_3	53 mg/g	(Choudhary et al., 2022)
2.	Polypyrrole/ Fe_3O_4 magnetic nanocomposite	22.3 mg/g	(Bhaumik et al., 2011)
3.	Mg-Al-Zr mixed oxides with calcium alginate beads (SA-CMAZ)	31.7 mg/g	(Wang et al., 2017)
4.	NiAl-layered metal oxide (NiAl-LMO)	49.28 mg/g	(Bai et al., 2019)
5.	single- and multi-walled carbon nanotubes	2.4/2.8 mg/g	(Dehghani et al., 2016)
6.	Activated carbon fibres modified with zirconium	8.86 mg/g	(Pang et al., 2020)
7.	Activated carbon/Iron	4.7 mg/g	(Sahu et al., 2021)
8.	Exhausted printer cartridge toner powder (PCt)	60 mg/g	Present study

As can be seen from Fig. 8, it can be understood that adsorption of fluoride on materials surface is majorly physical adsorption. Because this material has mesoporous properties it generates more active sites and provides more pore diffusion on it. At certain extent this study found that the PCt adsorbs fluoride through ion exchange, and surface complexation, by hydrogen bonding processes. Research suggests that the chemisorption of a single layer of molecules on an adsorbent surface is typically followed by further layers of physically adsorbed molecules from the adsorbate. The physisorption process is dominating in the adsorption process because the presence of carbon provides an abundance of surface complexation and electrostatic attraction to metal ions. Hence, the improved adsorption behavior can be explained by the physio-chemical interactions of fluoride species with PCt surface.

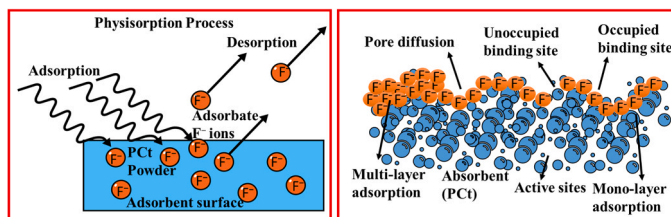


Fig. 8. Fluoride adsorption mechanism onto PCt powder.

5. Conclusion

The performance of the adsorption onto PCt powder was studied in the current study. At a pH of 7.0, with a contact period of 60 minutes and an adsorbent dose of 0.2 g, the adsorbent exhibited a percentage adsorption of 62% and a maximum adsorption capacity of 65 mg/g. The present study examined the equilibrium, kinetics, and thermodynamics of fluoride adsorption. The equilibrium data was analyzed using the Freundlich and Langmuir isotherm models, revealing a maximum adsorption capacity of 65 mg/g. The PCt powder has a morphology like cotton, accompanied by the presence of Fe₃O₄ spheres dispersed throughout. The rough and uneven surface of the material offers an increased number of active sites for the adsorption of fluoride. The adsorption process was found to conform to the pseudo-second-order model, as determined by kinetic investigations with PCt. This conclusion was supported by the close agreement between the theoretical and experimental sorption capabilities, as evidenced by a high coefficient of determination ($R^2 = 0.99$). After fluoride adsorption its characteristic data shows that it has no change in its structure and chemical composition, also it does not cause any elemental leaching in water. It can be recharged and reused 3 times after fluoride adsorption. This study shows that waste can be used to treat pollutant and can be reused multiple times. Fluoride treatment with PCt does not incur any expense and gives really great results for water treatment. Exhausted printer cartridges toner powder is first ever reported for fluoride treatment, is the best example of waste to wealth research.

Associated content

Supplementary data associated with this article is named supporting information file.

Declaration of Competing Interest

The authors declare that they have no known competing financial interests or personal relationships that could have appeared to influence the work reported in this paper.

Data Availability

Data will be made available on request.

Acknowledgments

Diksha Choudhary and Dr. Archana Singh would like to thank the Council of Scientific & Industrial Research (CSIR), New Delhi (grant number. 4/1/WTW/2023-IMD) and the Department of Science and Technology, Government of India (grant no. WTI/2K19/EWFH/2019/397) for their financial support of this work.

Appendix A. Supporting information

Supplementary data associated with this article can be found in the online version at [doi:10.1016/j.eti.2024.103572](https://doi.org/10.1016/j.eti.2024.103572).

References

- Akilarasan, M., Kogularasu, S., Chen, S.-M., Chen, T.-W., Lou, B.-S., 2018. A novel approach to iron oxide separation from e-waste and bisphenol A detection in thermal paper receipts using recovered nanocomposites. *RSC Adv.* 8 (70), 39870–39878. <https://doi.org/10.1039/C8RA08017H>.
- Arjunan, P., Kouthaman, M., Kannan, K., Diwakar, K., Priyanka, V., Subadevi, R., Sivakumar, M., 2021. Study on efficient electrode from electronic waste renewed carbon material for sodium battery applications. *J. Environ. Chem. Eng.* 9 (2), 105024. <https://doi.org/10.1016/j.jece.2021.105024>.
- Babar, S., Gavade, N., Shinde, H., Gore, A., Mahajan, P., Lee, K.H., Garadkar, K., 2019. An innovative transformation of waste toner powder into magnetic g-C₃N₄-Fe₂O₃ photocatalyst: sustainable e-waste management. *J. Environ. Chem. Eng.* 7 (2), 103041. <https://doi.org/10.1016/j.jece.2019.103041>.
- Bai, Z., Hu, C., Liu, H., Qu, J., 2019. Selective adsorption of fluoride from drinking water using NiAl-layered metal oxide film electrode. *J. Colloid Interface Sci.* 539, 146–151. <https://doi.org/10.1016/j.jcis.2018.12.062>.
- Bhaumik, M., Leswift, T.Y., Maity, A., Srinivasu, V.V., Onyango, M.S., 2011. Removal of fluoride from aqueous solution by polypyrrole/Fe₃O₄ magnetic nanocomposite. *J. Hazard. Mater.* 186 (1), 150–159. <https://doi.org/10.1016/j.jhazmat.2010.10.098>.
- Choudhary, D., Singh, A., Giri, A., Prasad, H.C., Sharma, R.K., Mishra, A., Singh, A., 2023. Functional hBN decorated Ni(OH)₂ nanosheets synthesized for remarkable adsorption performance for the elimination of fluoride ions. *Dalton Trans.* <https://doi.org/10.1039/d3dt01695a>.
- Choudhary, D., Tanwar, D., Gupta, D., Singh, P., Raizada, P., Singh, A., 2022. Disparate result of adsorptive removal of fluoride using manganese oxide-coated nano- γ -alumina oxide used with a different ratio. *IOP Conf. Ser.: Mater. Sci. Eng.* 1219 (1), 012032. <https://doi.org/10.1088/1757-899X/1219/1/012032>.
- Choudhary, D., Tavar, D., Singh, P., Raizada, P., Ashiq, M., Srivastava, A.K., Singh, A., 2022. Nanoalumina-supported Mn₂O₃ as efficient adsorbent for removal of fluoride and arsenic from water: a study from lab to field. *J. Mater. Sci.* 57 (28), 13326–13344. <https://doi.org/10.1007/s10853-022-07466-4>.
- Dehghani, M.H., Haghighat, G.A., Yetilmezsoy, K., McKay, G., Heibati, B., Tyagi, I., Gupta, V.K., 2016. Adsorptive removal of fluoride from aqueous solution using single- and multi-walled carbon nanotubes. *J. Mol. Liq.* 216, 401–410. <https://doi.org/10.1016/j.molliq.2016.01.057>.
- Dhillon, A., Kumar Sharma, T., Soni, S.K., Kumar, D., 2016. Fluoride adsorption on a cubical ceria nanoadsorbent: function of surface properties. *RSC Adv.* 6 (92), 89198–89209. <https://doi.org/10.1039/C6RA16962G>.
- Dong, L., Huang, Z., Ruan, J., Zhu, J., Huang, J., Huang, M., Zhang, T., 2017. Pyrolysis routine of organics and parameter optimization of vacuum gasification for recovering hazardous waste toner. *ACS Sustain. Chem. Eng.* 5 (11), 10038–10045. <https://doi.org/10.1021/acssuschemeng.7b02024>.

- Fernández, B., Ayala, J., Del Valle, E., Martínez-Blanco, D., Castañón, A.M., Menéndez-Aguado, J.M., 2022. Recycling of waste toner powder as adsorbent to remove aqueous heavy metals. *Mater. (Basel)* 15 (12). <https://doi.org/10.3390/ma15124150>.
- Hai, N., Phu, N., Luong, N., Chau, N., Chinh, H., Hoang, L., Leslie-Pelecky, D., 2008. Mechanism for sustainable magnetic nanoparticles under ambient conditions. In: *JOURNAL-KOREAN*, 52. PHYSICAL SOCIETY., p. 1327.
- Hammani, S., Barhoum, A., Nagarajan, S., Bechelany, M., 2019. Toner waste powder (TWP) as a filler for polymer blends (LDPE/HIPS) for enhanced electrical conductivity. *Mater. (Basel)* 12 (19). <https://doi.org/10.3390/ma12193062>.
- Itoua, P.I., Sun, D., Li, P., Shen, S., 2023. Influence of waste toner on asphalt binder: chemical and rheological characterization. *Molecules* 28 (6). <https://doi.org/10.3390/molecules28062794>.
- Kaipannan, S., Govindarajan, K., Sundaramoorthy, S., Marappan, S., 2019. Waste toner-derived carbon/Fe₃O₄ nanocomposite for high-performance supercapacitor. *ACS Omega* 4 (14), 15798–15805. <https://doi.org/10.1021/acsomega.9b01337>.
- Koochakzadeh, A., Alizadeh Gharetapeh, S., Jelodarian Bidgoli, B., 2022. Identification of pigments used in a Qajar manuscript from Iran by using atomic and molecular spectroscopy and technical photography methods. *Herit. Sci.* 10 (1), 30. <https://doi.org/10.1186/s40494-022-00665-x>.
- Kouser, M., Chowhan, B., Sharma, N., Gupta, M., 2022. Transformation of waste toner powder into valuable Fe₂O₃ nanoparticles for the preparation of recyclable Co (II)-NH₂-SiO₂@Fe₂O₃ and its applications in the synthesis of polyhydroquinoline and quinazoline derivatives. *ACS Omega* 7 (51), 47619–47633. <https://doi.org/10.1021/acsomega.2c04512>.
- Kumar, U., Gaikwad, V., Sahajwalla, V., 2018. Transformation of waste toner to iron using E-waste plastics as a carbon resource. *J. Clean. Prod.* 192, 244–251. <https://doi.org/10.1016/j.jclepro.2018.05.010>.
- Lou, Z., Huang, H., Li, M., Shang, T., Chen, C., 2013. Controlled synthesis of carbon nanoparticles in a supercritical carbon disulfide system. *Mater. (Basel)* 7 (1), 97–105. <https://doi.org/10.3390/ma7010097>.
- Nazlan, R., Ghazali, N.H., Nazri, N.A.A., Razali, A., Ramli, R.A., Lian, Y.M., 2022. Structural and magnetic characteristics evaluation of iron oxide extracted from printer toner wastes. *Mater. Sci. Forum* 1056, 99–104. <https://doi.org/10.4028/p-i4liyl>.
- Pang, T., Aye Chan, T.S., Jande, Y.A.C., Shen, J., 2020. Removal of fluoride from water using activated carbon fibres modified with zirconium by a drop-coating method. *Chemosphere* 255, 126950. <https://doi.org/10.1016/j.chemosphere.2020.126950>.
- Parthasarathy, M., 2021. Challenges and emerging trends in toner waste recycling: a review. *Recycling* 6 (3). <https://doi.org/10.3390/recycling6030057>.
- Peng, G.-h., Wang, X., Liang, Z.-h., Wang, Y.-c., Han, X.-b., Wu, J.-l., 2013. Preparation of spherical core-shell structured SiO₂@CaMoO₄:Eu³⁺,Li⁺ red phosphors. *J. Alloys Compd.* 576, 227–231. <https://doi.org/10.1016/j.jallcom.2013.04.127>.
- Pirela, S.V., Sotiriou, G.A., Bello, D., Shafer, M., Bunker, K.L., Castranova, V., Demokritou, P., 2015. Consumer exposures to laser printer-emitted engineered nanoparticles: a case study of life-cycle implications from nano-enabled products. *Nanotoxicology* 9 (6), 760–768. <https://doi.org/10.3109/17435390.2014.976602>.
- Raghav, S., Kumar, D., 2018. Adsorption equilibrium, kinetics, and thermodynamic studies of fluoride adsorbed by tetrametallic oxide adsorbent. *J. Chem. Eng. Data* 63 (5), 1682–1697. <https://doi.org/10.1021/acs.jced.8b00024>.
- Raghav, S., Sapna, Kumar, D., 2018. Cubical-shaped rods of pectin-hydroxyapatite composite for adsorption studies of fluoride by statistical method and adsorption experiments. *ACS Omega* 3 (8), 9675–9688. <https://doi.org/10.1021/acsomega.8b01330>.
- Rathore, V.K., Mondal, P., 2017. Competitive adsorption of arsenic and fluoride onto economically prepared aluminum oxide/hydroxide nanoparticles: multicomponent isotherms and spent adsorbent management. *Ind. Eng. Chem. Res.* 56 (28), 8081–8094. <https://doi.org/10.1021/acs.iecr.7b01139>.
- Sahu, N., Bhan, C., Singh, J., 2021. Removal of fluoride from an aqueous solution by batch and column process using activated carbon derived from iron infused Pisum sativum peel: characterization, Isotherm, kinetics study, 200241-200240 *Environ. Eng. Res.* 26 (4). <https://doi.org/10.4491/eer.2020.241>.
- Saini, D., Aggarwal, R., Anand, S.R., Sonkar, S.K., 2019. Sunlight induced photodegradation of toxic azo dye by self-doped iron oxide nano-carbon from waste printer ink. *Sol. Energy* 193, 65–73. <https://doi.org/10.1016/j.solener.2019.09.022>.
- Solanki, Y.S., Agarwal, M., Gupta, A.B., Gupta, S., Shukla, P., 2022. Fluoride occurrences, health problems, detection, and remediation methods for drinking water: a comprehensive review. *Sci. Total Environ.* 807, 150601. <https://doi.org/10.1016/j.scitotenv.2021.150601>.
- Solanki, Y.S., Agarwal, M., Gupta, S., Shukla, P., Maheshwari, K., Midda, M.O., 2019. Application of synthesized Fe/Al/Ca based adsorbent for defluoridation of drinking Water and its significant parameters optimization using response surface methodology. *J. Environ. Chem. Eng.* 7 (6), 103465. <https://doi.org/10.1016/j.jece.2019.103465>.
- Solanki, Y.S., Agarwal, M., Maheshwari, K., Gupta, S., Shukla, P., Gupta, A.B., 2020. Investigation of plausible mechanism of the synthesized inorganic polymeric coagulant and its application toward fluoride removal from drinking water. *Ind. Eng. Chem. Res.* 59 (20), 9679–9687. <https://doi.org/10.1021/acs.iecr.0c00760>.
- Talat, M., Mohan, S., Dixit, V., Singh, D.K., Hasan, S.H., Srivastava, O.N., 2018. Effective removal of fluoride from water by coconut husk activated carbon in fixed bed column: experimental and breakthrough curves analysis. *Groundw. Sustain. Dev.* 7, 48–55. <https://doi.org/10.1016/j.gsd.2018.03.001>.
- Wang, A., Zhou, K., Liu, X., Liu, F., Zhang, C., Chen, Q., 2017. Granular tri-metal oxide adsorbent for fluoride uptake: adsorption kinetic and equilibrium studies. *J. Colloid Interface Sci.* 505, 947–955. <https://doi.org/10.1016/j.jcis.2017.06.074>.
- Yordanova, D., Angelova, S., Dombalov, I., 2014. Utilisation options for waste toner powder. *J. Environ. Sci* 3, 140–144.
- Zhu, H., Zhou, Y., Wang, S., Wu, X., Hou, J., Yin, W., Yang, J., 2018. Preparation and application synthesis of magnetic nanocomposite using waste toner for the removal of Cr(vi). *RSC Adv.* 8 (49), 27654–27660. <https://doi.org/10.1039/C8RA05291C>.